Journal of Materials Chemistry C

ROYAL SOCIETY OF CHEMISTRY

PAPER

View Article Online
View Journal | View Issue

Cite this: J. Mater. Chem. C, 2023, 11, 4094

An efficient pink luminescent Eu(III) coordination polymer excited on a blue LED chip†

Nafisa A. Abusail, Najat Al Riyami, Rashid Ilmi, Muhammed S. Khan and Nawal K. Al-Rasbi *

Received 18th January 2023,
Accepted 20th February 2023

DOI: 10.1039/d3tc00215b

rsc.li/materials-c

Two new sets of lanthanide-based coordination polymers (CPs), $[Ln(DHTP)(NO_3)(H_2O)_4]_n$ [**Ln1** = **Gd1**, **Eu1**] and $[Eu_2(DHTP)(TTA)_4(DMF)_2(MeOH)_2]_n$ (**Eu2**) using 2,5-dihydroxyterephthalic acid (DHTP) and incorporating thenoyltrifluoroacetone (TTA) units, have been synthesized *via* condensation reactions and characterized. The single-crystal X-ray diffraction studies revealed that the **Eu1** CP has a 2D zig–zag chain while the **Eu2** CP exhibits a 2D polymeric structure derived from dinuclear Eu(III) building blocks. A detailed photoluminescence study proved that the band structure of the DHTP ligand is suitable for the luminescence sensitization of Eu(III). Efficient red emission is observed for the Eu(III) polymers in the solid state with a fairly large luminescence intrinsic quantum yield (Q_{Eu}) of 52% from the **Eu2** CP. Finally, a light emitting diode (LED) was fabricated by using a resin of 10% **Eu2** CP-silicon oil as the emitting layer over an InGaN blue LED chip. Interestingly, the **Eu2**/InGaN LED displays pink light with CIE 1931 chromaticity coordinates of (0.437, 0.185).

1. Introduction

Coordination polymer (CP) synthesis continues to stimulate research interests worldwide due to their potential for applications in a range of fields.[1] Among the plethora of metal ions, trivalent lanthanide [Ln(III)] ions remain at the forefront to synthesize lanthanide coordination polymers (LnCPs) due to their structural diversity and intriguing unique photophysical properties.[2–5] These properties include, but are not limited to, highly monochromatic photoluminescence (PL) (full width at half maxima (FWHM) = less than 10 nm), a large Stokes shift of the absorbed and emitted radiation, high PL quantum yield and a long luminescence lifetime (millisecond to microsecond). Moreover, a special property is the fingerprint PL (red PL for Eu(III), green PL for Tb(III), orange to deep red for Sm(III) *etc.*...) that covers the entire visible spectrum.[6] Thus, manipulation of PL colour could be achieved by just changing the Ln(III) ions without the use of expensive synthetic chemistry, which is needed when a transition metal ion is chosen. The LnCPs are designed and synthesised by self-assembly of a suitable organic "linker" with the Ln(III) metal ion into multi-dimensional solids.[7] In addition to their fascinating optical properties, LnCPs possess good chemical and thermal stability[8] with improved mechanical strength.[9] Because of these features, several LnCPs have been used in a range of applications such as sensors[10] and full-colour and white LEDs.[11]

Within the class of LnCPs, the Eu(III) CPs have attracted attention for red LEDs. Hasegawa and co-workers have developed a red phosphor excited by a blue LED.[12] The synthetic manipulation of red phosphors can be readily achieved by altering the organic linker(s).[13,14] First, the organic linker itself can act as an antenna, and because Eu(III) has a low-lying, first excited state of $^5D_0$ at 17 000 cm^{-1}, any organic linker with triplet state energy higher than 19 000 cm^{-1} can sensitize the Eu(III) centre efficiently and promote its emission quantum yields according to Latva's empirical rule.[15] Second, attachment of various functional groups such as hydroxyl, amino or nitro groups can alter the nature of the steric effects through variable hydrogen bonds (HBs) in the crystal lattice. This could lead to the formation of a tight 3D packed array of polymers that would suppress the non-radiative relaxation transitions about the Eu(III) centre. In addition, these packed arrays can enhance thermal stability of the polymers, making them suitable materials for LEDs.[16]

Ln(III) ions are hard acids and thus have a strong tendency to coordinate with hard bases. Due to the strong oxophilicity of Ln(III) ions,[17] many studies have focused on the linkers containing multi-carboxyl aromatic systems.[18,19] The multidentate carboxyl groups in the ligands provide abundant coordination modes with Ln(III) that lead to variable structures and luminescence properties.[20] In the present work, we have utilized DHTP as a prime organic antenna moiety to design and synthesize a

Department. of Chemistry, College of Science, Sultan Qaboos University, Al-Khode 123, Oman. E-mail: nrasbi@squ.edu.om; Fax: +968 24141469

† Electronic supplementary information (ESI) available. CCDC 2204043–2204044. For ESI and crystallographic data in CIF or other electronic format see DOI: https://doi.org/10.1039/d3tc00215b

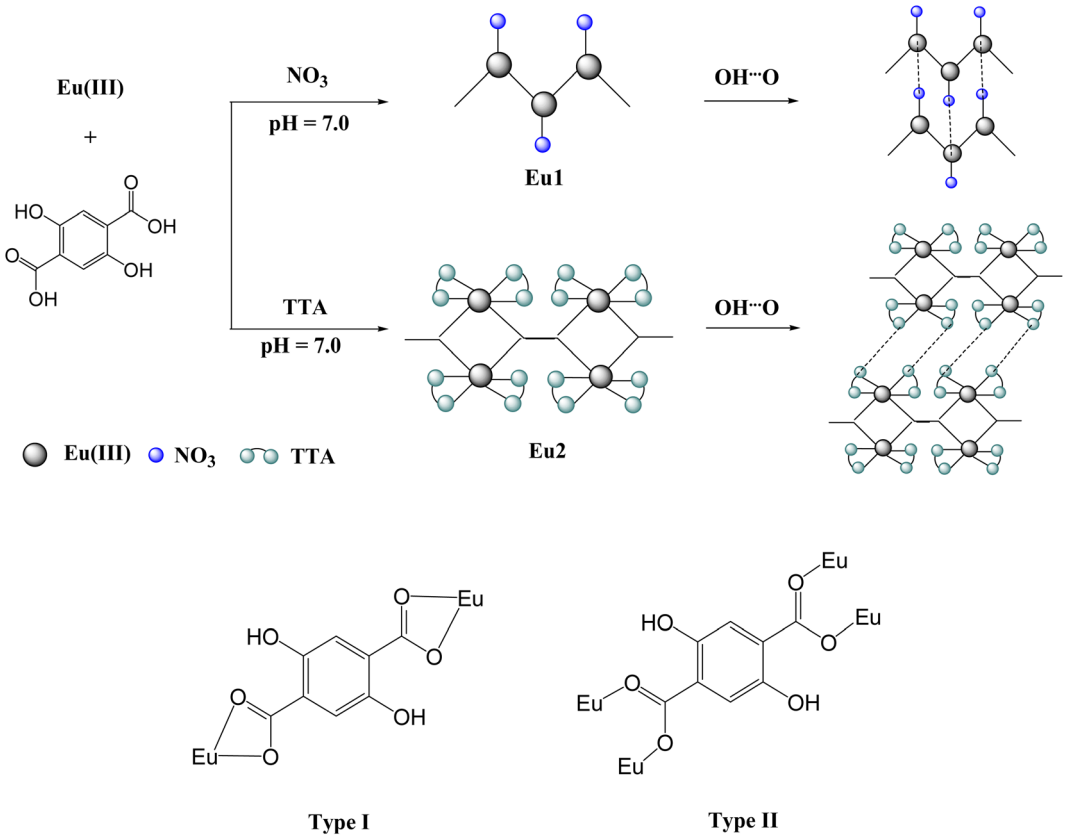

Scheme 1 The synthetic routes for the coordination polymers: **Eu1** and **Eu2**. Bottom: The different coordination modes of the DHTP ligand.

novel class of Eu(III) CPs of the general formula: $[Eu(DHTP)(NO_3)(H_2O)_4]_n$ (**Eu1**) (Scheme 1). Long-range non-covalent interactions (NCI) such as inter- and intra-molecular HB interactions play a central role in supramolecular chemistry and molecular recognition.[21,22] In the DHTP linker, there are two hydroxyl groups at 2 and 5 positions that could be involved in inter- and intra-molecular HB interactions to form 2D and 3D supramolecular structures, which is indeed the case as determined using single crystal X-ray diffraction studies (*vide supra*). Moreover, HB interactions could be beneficial in improving the PL properties by suppressing the non-radiative relaxation transitions.[23,24] Furthermore, the supramolecular structures formed through the HB effect could trigger other NCIs such as $\pi\cdots\pi$ interactions (*vide supra*)[25] and will certainly be helpful in improving the thermal stability, energy migration and electron transport properties.[24] Moreover, the presence of water and solvent molecule(s) in the inner-coordination sphere has a detrimental effect on the PL processes due to vibronic coupling. Nevertheless, this can be overcome by replacing them with additional suitable ligand(s). One of the ligands of choice is "β-diketone" that has dominated the lanthanide coordination chemistry. We have employed TTA as an ancillary ligand to synthesize another set of Eu(III) CPs with the formula: $[Eu_2(DHTP)(TTA)_4(DMF)_2(MeOH)_2]_n$ (**Eu2**). The presence of TTA would result in chemically and thermally stable **Eu2** CPs due to the presence of hard donor oxygen atoms with favourable triplet states, especially for Eu(III), improving the PL properties of polymers. The photophysical properties of the Eu(III) CPs were analysed in detail by means of excitation and emission time-resolved spectroscopy. The effect of the bonding ancillary ligand in the present LnCPs has been discussed in detail by correlating with the Judd–Ofelt (Ω_2 and Ω_4) intensity parameter, radiative (k_R) and non-radiative (k_{NR}) decay rates, and radiative lifetime (τ_r). Encouraged by the interesting photophysical properties, we doped the **Eu2** CP onto a lnGaN blue LED device. The fabricated device displayed pink emission with CIE coordinates of x = 0.41 and y = 0.18.

2. Experimental section

General details

All organic reagents, metal salts and solvents were purchased from commercial suppliers and used as received without further purification. Infrared spectra were recorded using KBr pellets on a PerkinElmer FT–IR spectrometer BX in the range of 4000–400 cm^{-1}. Electrospray (ES) mass spectra were recorded on a VG Autospec magnetic sector instrument. Elemental analysis for carbon, hydrogen and nitrogen was performed using the PerkinElmer 2400 CHNS/O Series II Elemental Analyser.

Synthesis of Ln1 CPs (Eu1 and Gd1)

The general procedure of preparing **Ln1** CPs involves reacting $Ln(NO_3)_3{\cdot}xH_2O$ (Ln = Eu or Gd) salts with the ligands in a 1 : 1

molar ratio in the presence of MeOH/water. The mixture was refluxed for 4 hours at 100 °C. For example, DHTP (0.050 g, 0.25 mmol) was dissolved in a mixture of MeOH (10 mL) and water (30 mL) and refluxed for 30 minutes. The pH of the solution was adjusted to 7 by the addition of a few drops of dilute NH_3. Then $Eu(NO_3)_3{\cdot}5H_2O$ (0.10 g, 0.25 mmol) dissolved in 2 mL of water was added dropwise to the previous solution. The mixture was stirred at 100 °C for 4 hours and then cooled to RT. Colorless crystals formed, which were filtered and washed with MeOH. The polymers are air and moisture stable solids, and their characterization data are as follows:

$[Eu(DHTP)(NO_3)(H_2O)_4]_n$ (Eu1)

Colorless blocks. Yield 80%. $EuC_8H_{12}N_1O_{13}$ (482.08) Exp (calc): %C 20.01 (19.93), %H 2.43 (2.50), %N 2.72 (2.90); ESI-MS *m*/*z* 567.2 $\{[Eu(DHTP)_2H_2O]\}^+$, 432 $\{[Eu(DHTP)(NO_3)\ H_2O]\}^+$, and 646 $\{[Eu(DHTP)_2(NO_3)(H_2O)]\}$ (Fig. S1, ESI†). FT-IR cm^{-1} (solid): 3345, 2960, 1590, 1506, 798.

$[Gd(DHTP)_2(NO_3)(H_2O)_4]_n$ (Gd1)

Colorless blocks. Yield is 80% of yellow powder. $GdC_8H_{12}N_1O_{13}$ (487.43) Exp (calc): C% 19.63 (19.69), H% 2.45 (2.48), N% 2.79 (2.86); ESI-MS *m*/*z*: 633 $\{[Gd(DHTP)_2(NO_3)(H_2O)]\}^+$, 651 $\{[Gd(DHTP)_2(NO_3)(H_2O)_2]\}^+$.

Synthesis of Eu2 CP

The general procedure of preparing the **Eu2** polymer involved reacting $EuCl_3{\cdot}6H_2O$, DHTP and TTA in a molar ratio of 1 : 1:2 in MeOH/DMF at pH 7. For example, TTA (0.23 mmol, 0.050 g) and $EuCl_3{\cdot}6H_2O$ (0.040 g) were dissolved in MeOH (7 mL) and water (5 mL). The pH was adjusted to 7 by the addition of dilute NH_3 solution. After stirring for 30 min at 80 °C, DHTP (0.11 mmol, 0.020 g) was added. The reaction mixture was stirred at 100 °C for 2 hours. DMF (2 mL) was added and the reaction mixture was left to cool at room temperature. Pale yellow crystals formed overnight. The solid was filtered off and washed with MeOH. The **Eu2** polymer is an air and moisture stable solid, and its characterization data are as follows:

$[Eu_2(DHTP)(TTA)_4(DMF)_2(MeOH)_2]_n$ (Eu2)

Pale yellow blocks. Yield 78%. $EuC_{24}H_{23}N_1O_{10}F_6S_2$ (815.32) exp (calc): C% 35.39 (35.36), H% 2.77 (2.84), N% 1.79 (1.72) ESI-MS *m*/*z*: 836.25 $\{[Eu(DHTP)(TTA)_2(DMF)\text{-}(MeOH)][(H_2O)\}^+$ and 1654.25 $\{[Eu_2(DHTP)(TTA)_4(DMF)_2(MeOH)_2][(H_2O)_2\}^+$. FT-IR cm^{-1} (solid): 3237, 1599, 2930, 1124, 1247 and 680.

Single crystal X-ray diffraction analyses

Single crystals of **Eu1** and **Eu2** were obtained as detailed above and the data were collected at 150 K, using a STOE IPDS II diffractometer equipped with Mo-K_α radiation. The sample temperature was controlled using an Oxford Diffraction Cryojet apparatus. Data were integrated using the Stoe X-AREA[26] software package. The numerical absorption coefficient, μ, for MoKα radiation is 7.383. The numerical absorption correction was applied using the X-RED software package.[27] The data were corrected for Lorentz and Polarizing effects. The structures were solved using direct methods and subsequent difference Fourier maps and then refined on F^2 by a full-matrix least-squares procedure using anisotropic displacement parameters with SHELXS-97.[28] All of the hydrogen atoms were positioned geometrically in idealized positions and refined with the riding model approximation, with $U_{iso}(H) = 1.2$ or $1.5U_{eq}(C)$. All the refinements were performed using the WinGX[29] suite of programs. For the molecular graphics the program Mercury package was used.[30] The non-hydrogen atoms were refined anisotropically. In $[Eu_2(DHTP)(TTA)_4(DMF)_2(MeOH)_2]_n$ (**Eu2**), the carbon atom C22 from the TTA unit is disordered and was refined as isotropic to keep the refinement stable. Comments on the checkcif files can be found in detail in the supplementary information.

Photophysical measurements

UV-visible absorption spectra were recorded on a Varian Cary 5000 UV-visible spectrophotometer in the 250–800 nm range. Quartz cuvettes of 1 cm path length were used and solvent background corrections were applied. Steady state emission spectra and phosphorescence lifetimes (τ_{obs}) for Eu(III) f–f transitions in the solid state were recorded on an Edinburgh FS5 fluorimeter at RT. The lifetimes were measured by recording the decay at the maximum of the emission spectra. The goodness of the fits was judged by the value of the reduced chi-squared (χ^2). The triplet state energy of DHTP was recorded from its Gd(III) polymer in ethanol (1×10^{-5} M) at 77 K using an NMR tube. Important photophysical parameters such as Judd–Ofelt (J–O) parameters (Ω_2 and Ω_4), radiative (k_R) and non-radiative (k_{NR}) decay rates, radiative lifetime (τ_r) and intrinsic quantum yield (Q_{Eu}^{Eu}) were calculated using the following eqn (1)–(6) and details were reported elsewhere.[31]

$$\Omega_\lambda^{exp} = \frac{3\hbar k_R\left[^5D_0 \rightarrow {}^7F_J\right]}{32e^2\pi^3\chi\nu\left[^5D_0 \rightarrow {}^7F_J\right]^3\left|\langle {}^5D_0\|U^{(\lambda)}\|{}^7F_J\rangle\right|^2} \quad (1)$$

$$k_R = \sum_{J=0}^{4} k_R\left[^5D_0 \rightarrow {}^7F_J\right] \quad (2)$$

$$k_R\left[^5D_0 \rightarrow {}^7F_J\right] = \frac{\nu\left[^5D_0 \rightarrow {}^7F_1\right]}{\nu\left[^5D_0 \rightarrow {}^7F_J\right]} \times \frac{A\left[^5D_0 \rightarrow {}^7F_J\right]}{A\left[^5D_0 \rightarrow {}^7F_1\right]} k_R\left[^5D_0 \rightarrow {}^7F_1\right] \quad (3)$$

$$\tau_r = 1/k_R \quad (4)$$

$$k_{NR} = \frac{1}{\tau_{obs}} - \frac{1}{\tau_r} \quad (5)$$

$$Q_{Eu} = \frac{\tau_{obs}}{\tau_r} = \frac{k_R}{k_R + k_{NR}} \quad (6)$$

Fabrication of a LED package

An InGaN blue LED as a side-view type LED package (Nichia Corporation) was fabricated. A silicon resin with 10% of **Eu2** CP was doped on the surface of the blue LED.

3. Results and discussion

3.1 Synthesis, characterization and thermal analysis of Eu1 CP

New Ln(III) CPs, where Ln is Eu and Gd with DHTP, have been successfully synthesized and their structures were established by single crystal X-ray diffraction, elemental analysis, infrared spectra and thermogravimetric analysis. The synthetic routes for the polymers are presented in Scheme 1. The first set of polymers, **Ln1**, was obtained from the reaction of Ln(III) nitrate salts with DHTP in a 1 : 1 molar ratio in aqueous media at pH 7. After a couple of hours under reflux, the polymers started to precipitate. Crystals from $[Eu(DHTP)(NO_3)(H_2O)_4]_\infty$ (**Eu1**) were successfully obtained by solvent diffusion within a few minutes. **Eu1** CP exhibits a 2D zig–zag chain in a 2D network. However, another set of Ln(III) CPs has been designed by the incorporation of TTA units to afford further protection for the Ln(III) centre from coordinating water molecules. $EuCl_3{\cdot}6H_2O$, DHTP and TTA moieties were reacted in a molar ratio of 1 : 1 : 2 in a mixture of MeOH and DMF at pH 7. Sharp needles of the CP: $[Eu_2(DHTP)(TTA)_4(DMF)_2(MeOH)_2]_n$ (**Eu2**) were obtained by the slow evaporation of the reaction mixture within a few hours. The second polymer, **Eu2**, is based on dinuclear Eu(III) building blocks that exhibit a different 2D chain of polymers.

Infrared results

The solid-state infrared spectra (IR) of DHTP and its CPs were investigated (Fig. S2, ESI†). For DHTP, a strong stretching band of O–H attributed to the carboxylic acid and alcohol is observed at 3450 cm^{-1}; and a carbonyl (C═O) band attributed to the acid is observed at 1638 cm^{-1}. However, to determine the coordination mode of the carboxylate group, one can use the equation:[32]

$$\Delta\upsilon_{as-s} = [\upsilon_{as}(COO) - \upsilon_{s}(COO)]$$

where $\upsilon_{as}(COO)$ and $\upsilon_{s}(COO)$ are, respectively, the asymmetric and the symmetric stretching of C═O in the carboxylic acid. Generally, if the stretching difference $\Delta\upsilon_{as-s}$ value is less than 200 cm^{-1}, it is believed that COO^- adopts the bidentate and bridging mode. If the $\Delta\upsilon_{as-s}$ value is greater than 200 cm^{-1}, it is believed that the COO^- adopts the monodentate mode. In the IR spectra of the Ln(III) CPs, the calculated $\Delta\upsilon_{as-s}$ value is less than 200 cm^{-1} for the coordinating DHTP. For example, for **Eu1**, the asymmetric stretching vibration peak of the COO^- groups is located at 1590 cm^{-1}, while the symmetric stretching vibration absorption peak appeared at 1506 cm^{-1}. The calculated $\Delta\upsilon_{as-s}$ value is 84 cm^{-1}. These results confirm that the COO^- groups adopt the bidentate chelating mode by bridging the two Ln(III) centres in all sets of CPs. In addition, the CPs exhibit a broad band centered at around 3300 cm^{-1} confirming

Table 1 Crystal data and structure refinement for **Eu1** and **Eu2** CPs

Identification code	**Eu1**	**Eu2**
Empirical formula	$C_8H_{12}EuNO_{15}$	$C_{24}H_{20}EuF_6NO_9S_2$
Formula weight	514.14	796.49
Temperature	150(2) K	150(2) K
Wavelength	0.71073 Å	0.71073 Å
Crystal system	Monoclinic	Monoclinic
Space group	$P2_1/c$	$P2_1/n$
a	15.460(3) Å	9.990(2) Å
b	6.4600(13) Å	19.280(4) Å
c	15.470(3) Å	15.570(3) Å
α	90°	90°
β	90.10(3)°	90.30(3)°
γ	90°	90°
Volume	1545.0(5) $Å^3$	2998.9(10) $Å^3$
Z	4	4
Density (calculated)	2.210 Mg m^{-3}	1.760 Mg m^{-3}
Absorption coefficient	4.144 mm^{-1}	2.317 mm^{-1}
F(000)	1000	1560
Crystal size	0.200 × 0.200 × 0.100 mm^3	0.180 × 0.160 × 0.050 mm^3
Theta range for data collection	2.633 to 26.356°	2.428 to 27.497°
Index ranges	$-17 \le h \le 19$, $-8 \le k \le 8$, $-19 \le l \le 19$	$-12 \le h \le 12$, $-23 \le k \le 25$, $-20 \le l \le 20$
Reflections collected	11687	27796
Independent reflections	3137 [R(int) = 0.1054]	6863 [R(int) = 0.0592]
Completeness to theta = 25.242°	99.8%	99.9%
Refinement method	Full-matrix least-squares on F^2	Full-matrix least-squares on F^2
Data/restraints/parameters	3137/8/218	6863/209/442
Goodness-of-fit on F^2	1.266	1.152
Final R indices [$I > 2$sigma(I)]	R_1 = 0.06608, wR_2 = 0.1594	R_1 = 0.0644, wR_2 = 0.1502
R indices (all data)	R_1 = 0.0951, wR_2 = 0.1754	R_1 = 0.0756, wR_2 = 0.1566
Extinction coefficient	0.0013(4)	0.0038(4)
Largest diff. peak and hole	3.826 and −2.625 e^{-3}	1.631 and −1.818 e $Å^{-3}$
CCDC deposition number	2204044	2204043

the presence of OH units of DHTP protonated and uncoordinated to the metal centres.

Thermogravimetric analysis

The thermal stability of the Ln(III) CPs has been investigated using thermogravimetric analysis, TGA. Fig. S3 (ESI†) shows the thermogram of **Eu2** recorded under an inert N_2 atmosphere. The TGA curve gives a good indication of the stability of the polymer up to 170 °C. In fact, the first decomposition process occurs between 170–360 °C as the TTA units are lost with a weight loss of 51.1%, calc (52.1%). The second weight loss takes place between 360–1150 °C as the main coordination polymer [Eu(DHTP)] decomposes with a weight loss of 26.6%, calc (27.2%). Finally, the last decomposition step corresponds to the residual europium oxide with a weight loss of 22.1%, calc (21.7%). We observed similar behaviour for other **Ln1** CPs.

3.2 Analysis of single crystal X-ray structures

Crystal structure of Eu1. Crystals from $[Eu(DHTP)(NO_3)(H_2O)_4]_\infty$ (**Eu1**) crystallize in the monoclinic space group $P2_1/c$. The important crystallographic data and structure refinement for all the Ln(III) complexes reported herein are listed in Table 1. X-ray diffraction studies reveal a 1D zig–zag polymer of **Eu1** assembled from $DHTP^{2-}$ and $Eu(NO_3)^{2+}$ units. The asymmetric unit of **Eu1** contains one Eu(III) centre coordinating to one $DHTP^{2-}$ ligand, one nitrate ion and 8 water molecules. Each Eu(III) centre is in a 9-coordinate environment, with four carboxylate oxygen atoms (O^5, O^6, O^7 and O^8) derived from two bridging DHTP ligands, and another four oxygen atoms (O^1, O^2, O^3 and O^4) from four aqua molecules and one oxygen atom (O^9) from the nitrate ion, Fig. 1(a). The EuO_9 coordination polyhedron can be described as a capped square-antiprism with approximate C_2-symmetry around the metal centre. The bond distances to the Eu(III) center are comparable to those of previously published Eu(III) CPs from carboxylate units.[33] The $Eu–O_{carboxylate}$ bond length is in the range of 2.480(7)–2.508(8) Å (Table 2); the $Eu–O_{nitrate}$ bond length is 2.535(7) Å; and the $Eu–O_{aqua}$ bond length is in the range of 2.372(7)–2.422(8) Å. The angle between the two Eu(*OCO*) planes is 81.78° identified by atoms: C1, **Eu1** and C5.

Interestingly, DHTP adopts the coordination mode of type **I** (Scheme 1) to bridge two Eu(III) centres to form an infinite 2D zig–zag chain as shown in Fig. 1b. The calculated Eu···Eu separation is 11.518 Å. The alcohol group (–OH) of DHTP does not participate in coordination to the Eu(III) centre, but is involved in the formation of hydrogen interactions of O15–H···O15′ and O16–H···O16′ between the alcohol groups on both sides of the adjacent zigzag chains of **Eu1** to link the 2D chains into 2D supramolecular zigzag sheets (Fig. 1c). The distances of the hydrogen interactions in these contacts are 3.113 and 3.314 Å respectively. There are other O–H···O contacts that also play an important role in stabilizing the architecture which have been identified between the aqua ligands and the COO units. For example, the O2–H···O5 contact is found to be 2.772 Å. As expected, the 3D supramolecular zig–zag sheets of **Eu1** are packed in an ABAB sequence along the *a*-axis direction.

We also synthesised a **Gd1** CP with **DHTP**. All of the spectroscopic and analytical data confirmed the formulation of the CP: $[Gd(DHTP)(NO_3)(H_2O)_4]_n$ (**Gd1**).

Crystal structure of Eu2

The crystal structure of the **Eu2** CP exhibits a 2D coordination polymer derived from dinuclear Eu(III) building blocks, Fig. 2. The asymmetric unit contains one independent Eu(III) centre in an 8-coordinate environment, which is bonded to two

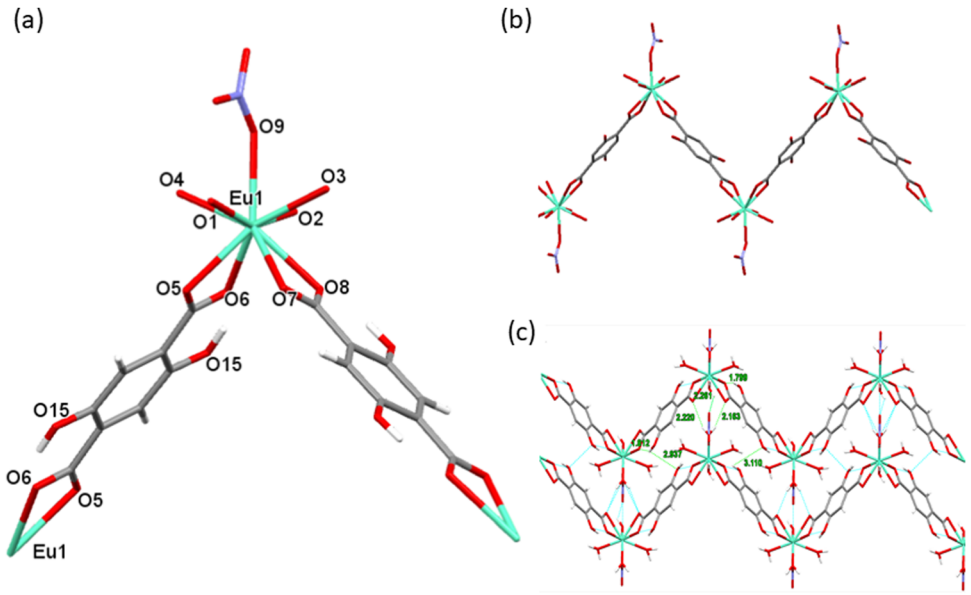

Fig. 1 (a) Presentation of the coordination sphere of Eu(III) in **Eu1**. (b) View of the two-dimensional infinite zig–zag chain formed by **Eu1** CP. (c) View of the 3D supramolecular zigzag sheets formed by **Eu1** CP.

Table 2 Bond lengths [Å] and angles [°] for **Eu1**

Eu(1)–O(1)	2.376(9)	Eu(1)–O(6)	2.475(9)
Eu(1)–O(2)	2.365(9)	Eu(1)–O(7)	2.512(10)
Eu(1)–O(3)	2.412(10)	Eu(1)–O(8)	2.486(9)
Eu(1)–O(4)	2.411(10)	Eu(1)–O(9)	2.536(9)
Eu(1)–O(5)	2.496(9)		
O(2)–Eu(1)–O(3)	85.5(3)	O(2)–Eu(1)–O(7)	122.7(3)
O(1)–Eu(1)–O(3)	85.0(3)	O(1)–Eu(1)–O(7)	76.6(3)
O(4)–Eu(1)–O(3)	134.5(3)	O(4)–Eu(1)–O(7)	144.9(3)
O(2)–Eu(1)–O(6)	71.3(3)	O(3)–Eu(1)–O(7)	73.6(3)
O(1)–Eu(1)–O(6)	127.8(3)	O(6)–Eu(1)–O(7)	93.6(3)
O(3)–Eu(1)–O(6)	141.8(3)	O(8)–Eu(1)–O(7)	51.7(3)

Table 3 Bond lengths [Å] and angles [°] for **Eu2**[a]

Eu(1)–O(1)	2.339(5)	Eu(1)–O(6)	2.304(6)
Eu(1)–O(2)	2.362(5)	Eu(1)–O(7)	2.325(6)
Eu(1)–O(1M)	2.445(6)	Eu(1)–O(8)	2.370(6)
Eu(1)–O(5)	2.365(6)	Eu(1)–O(9)	2.392(6)
O(6)–Eu(1)–O(7)	87.6(2)	O(7)–Eu(1)–O(8)	72.1(2)
O(6)–Eu(1)–O(1)	106.3(2)	O(1)–Eu(1)–O(8)	140.8(2)
O(7)–Eu(1)–O(1)	146.1(2)	O(2)#1–Eu(1)–O(8)	73.1(2)
O(6)–Eu(1)–O(2)#1	142.7(2)	O(5)–Eu(1)–O(8)	135.1(2)
O(7)–Eu(1)–O(2)#1	100.6(2)	O(6)–Eu(1)–O(9)	76.1(2)
O(1)–Eu(1)–O(2)#1	86.9(2)	O(7)–Eu(1)–O(9)	145.9(2)

[a] Symmetry transformations used to generate equivalent atoms: #1 $-x+1, -y+1, -z+1$ and #2 $-x+2, -y+1, -z+1$.

carboxylate oxygen atoms from two bridging DHTP ligands, four oxygen atoms from two TTA units, one oxygen atom from DMF and one oxygen atom from a methanol molecule. The EuO_8 coordination polyhedron has the geometry of a distorted square antiprism, with approximate C_2-symmetry around the metal centre. The bond distances to the Eu(III) centre are comparable to those of known Eu(III) polymers with ligands that adopt similar coordination modes.[34] As summarized in Table 3, the Eu–$O_{carboxylate}$ bonds are in the range of 2.340(6)–2.364(7) Å, Eu–O_{TTA} bonds are in the range of 2.302(7)–2.368(7) Å; and the Eu–O_{DMF} bond length is 2.397(7) Å. The angle between the two Tb(*OCO*) planes is 79.90°.

Compared with **Eu1**, DHTP adopts a different coordination mode of type **II** to connect the Eu(III) centers (Scheme 1). Each building block contains two Eu(III) centres linked together by one carboxylate unit from one side of DHTP (Fig. 2b). So, within the di-nuclear building block, the Eu···Eu separation is 5.224 Å. The adjacent building blocks connect to each other by one carboxylate unit from the other side of DHTP resulting in the formation of a two-dimensional polymer as shown in Fig. 2c. The polymer exhibits π···π stacking interactions of 3.698 Å between the DHTP and the thenoyl rings that are responsible for the stability of the polymer. The Eu···Eu separation between two successive building blocks is 12.045 Å. In addition, each building block exhibits variable H-bonding interactions of OH···O(TTA) (2.667 Å) and (DHTP) CH···O(TTA) (2.932 and 3.558 Å). Finally, the parallel chains of polymers are packed together through CH···F contacts that results in the formation of 3D supramolecular sheets, Fig. 2d.

4. Photophysical properties

The UV/Vis absorption spectrum of the free DHTP was determined in dilute tetrahydrofuran solution (10^{-5} M) and is shown in Fig. S4 (ESI†). The spectrum displayed a strong π–π* transition λ_{max}^{abs} = 374 nm with a molar absorption coefficient (ε) of

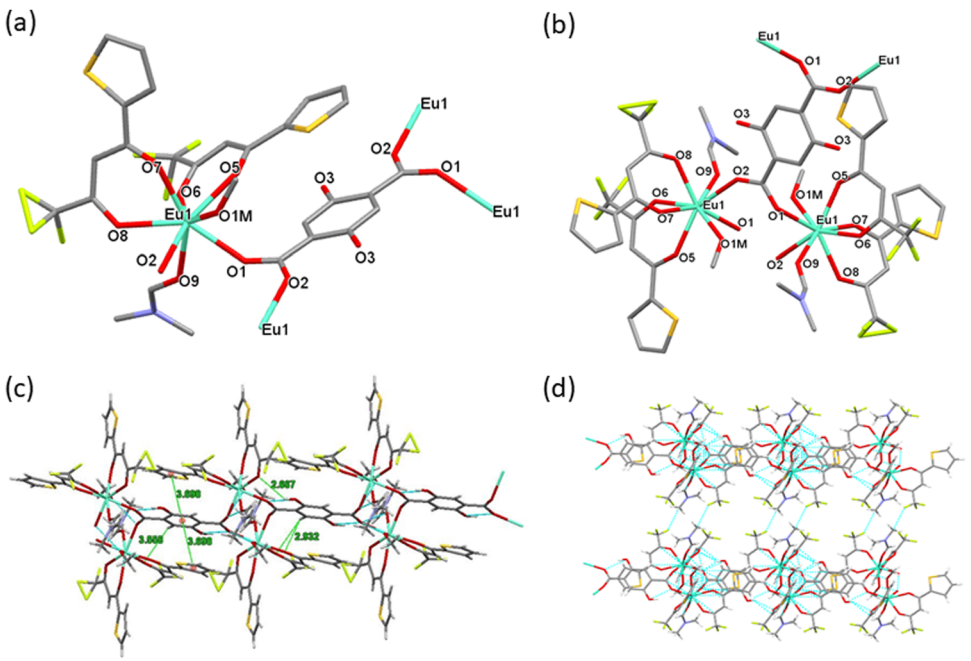

Fig. 2 (a) The asymmetric unit of **Eu2**. (b) Presentation of the dinuclear Eu(III) building blocks in **Eu2**. (c) View of the **Eu2** polymer. (d) View of the 3D supramolecular sheets formed by the **Eu2** CP.

26 000 M^{-1} cm^{-1} implying that the organic linker has a good light absorbing capability. The Ln CPs are not soluble in common solvents and their absorption spectra are not recorded in solution.

Apart from the light absorbing capability, an important parameter of efficiently emitting lanthanide material is energy matching between the triplet band energy (T_1) of the chelating organic ligand and the emitting state of the Ln(III) ion in question. Generally, in CPs, the organic linker DHTP would most likely behave as an aggregated organic compound with band-network structures rather than a single molecule.[35] Upon coordination to the Ln(III) centre, the triplet state energy of the band is responsible for the sensitization process. Thus, the triplet band energy (T_1) of DHTP can be determined experimentally from the phosphorescence spectrum of its isostructural Gd(III) CP recorded in ethanol at 77 K. Generally, Gd(III) complexes are optimal for this purpose due to the large probability of the phosphorescence because of the combination of both paramagnetic[36] and heavy atom effects. Moreover, $^6P_{7/2}$ of Gd(III) lies at 32 000 cm^{-1}, which is too high to be populated by most of the organic ligands.[37] Therefore, we synthesized a new **Gd1** CP (please see the Experimental section) and measured its phosphorescence spectrum at 77 K and fluorescence spectrum at room temperature (Fig. S5, ESI†). From the 77 K phosphorescence spectrum of **Gd1**, T_1 of the DHTP is calculated which is equal to 21 800 cm^{-1} (458 nm) and is comparable to that of related terephthalate ligands reported previously.[38] The energy gap (ΔE) between T_1 and $^5D_0$ falls within the range suggested by Latva's rule,[39,40] ΔE = 4500 cm^{-1}, highlighting the efficiency of Eu-CPs. Moreover, according to Reinhoudt's empirical rule,[41] the intersystem crossing (ISC) process becomes effective if the energy difference, $\Delta E(S_1 - T_1)$, is around 5000 cm^{-1}. To check this, we have also calculated the singlet state energy (S_1) of DHTP which is 27 000 cm^{-1} (370 nm) with the $\Delta E(S_1 - T_1) \approx 5200$ cm^{-1} implying effective ISC in the sensitization process, Fig. S6 (ESI†).

The steady-state PL spectra of Eu(III) CPs were investigated in detail in the solid-state at room temperature, Fig. 3, and are summarized in Table 4. Upon excitation, the CPs exhibited typical Eu(III) emission transitions originating from the $^5D_0$ excited state to the ground mutiplets: $^7F_{0-4}$. The spectra in each case are dominated by the electric-dipole $^5D_0 \rightarrow {}^7F_2$ transitions. It has been well documented that the ratio between the relative intensity of the magnetic-dipole and electric-diploe transitions *i.e.* $R_{21} = I(^5D_0 \rightarrow {}^7F_2)/I(^5D_0 \rightarrow {}^7F_1)$ (I = integrated emission intensity of the corrected emission spectrum) can be used as a criterion for the symmetry distortion of the Eu(III) ion's nearest surroundings. The high value of $R_{21} \approx 10.28$ and 12.70, respectively, for **Eu1** and **Eu2** suggests that the surroundings around the Eu(III) ion in the CPs are non-centrosymmetric, with a low symmetry of the crystal field (C_2) for the Eu(III) centre in 8-coordinate and 9-coordinate geometries in agreement with their X-ray crystal structures.[42] Moreover, the higher total integral intensity of $^5D_0 \rightarrow {}^7F_2$ transition compared to $^5D_0 \rightarrow {}^7F_1$ also indicates that the forced electric dipole and the dynamic coupling mechanism are dominant over magnetic dipoles.[42]

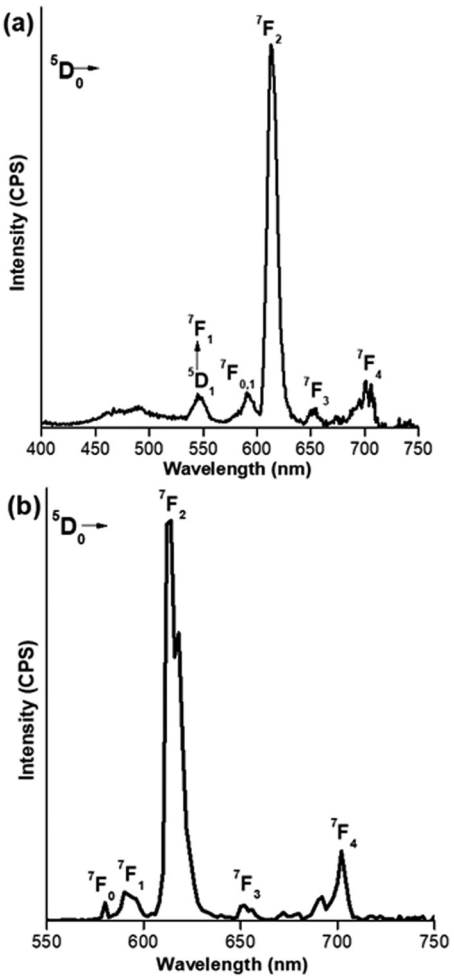

Fig. 3 Room temperature solid-state PL spectra of the **Eu-CPs**: (a) **Eu1** (excited at 370 nm) and (b) **Eu2** (excited at 345 nm).

The CIE (Commission Internationale de l'Eclairage) coordinates are used to characterize the color and location of all the color coordinates produced within the limit of the CIE chromaticity diagram. The CIE color coordinates of Eu-CPs are shown in Fig. 4. The CIE color coordinates of **Eu1** fall in the orange region while **Eu2** displays typical red emission with CIE color coordinates very close to the National Television System Committee (NTSC) (0.668, 0.325) and thus **Eu2** could be a promising candidate as a red component for the fabrication of LEDs.[43] The orange emission of **Eu1** could be due to the presence of residual ligand fluorescence, which arose because of the presence of water/DMF molecules in the inner coordination sphere that deactivates the excited state non-radiatively.

To further understand the extent of participation of the non-radiative process in both Eu(III) CPs, we utilized time-resolved spectroscopy and determined the $^5D_0$ excited state lifetime (τ_{obs}). τ_{obs} was determined by fitting the decay curves in Fig. S7 (ESI†). As expected **Eu1** displayed an 8.46 fold shorter τ_{obs} value than **Eu2**. To clearly understand, we have utilized the steady-state emission spectra and τ_{obs} to calculate important photophysical parameters such as the radiative decay rate (k_R),

Table 4 Summary of the experimental photophysical parameters of the Eu(III) CPs at RT

	Ω_2 $\times 10^{-20}$ cm^2	Ω_4	FWHM (nm)	τ_{obs} (μs)	τ_r^c (μs)	K_R (s^{-1})	K_{NR} (s^{-1})	Q_{Eu}	R_{21}	CIE$_{(x,y)}$
Eu-1	18.05	6.29	11.01	78.00	1463	683.58	12136.93	5.33	10.28	(0.518, 0.340)
Eu-2	22.29	8.50	8.78	600	1756	869.39	797.27	52.16	12.70	(0.668, 0.325)

Ω_2 and Ω_4 were calculated by applying eqn (1) and (2). K_R and k_{NR} were calculated by applying eqn (2) and (4). Q_{Eu} was calculated by applying eqn (6).

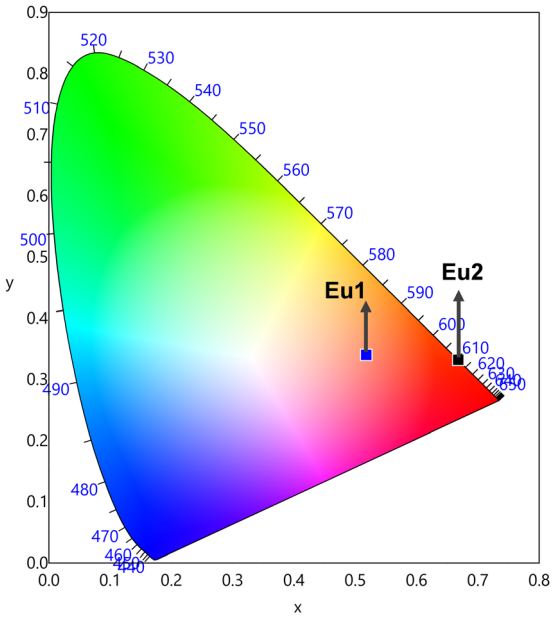

Fig. 4 The CIE 1931 chromaticity diagram of the Eu(III) CPs in the solid-state.

non-radiative decay rate (k_{NR}) and the intrinsic quantum yield of the Eu(III) centre, Q_{Eu}. The Ω2 and Ω_4 values were also calculated by applying the mathematical eqn (1)–(6). All the obtained data are summarized in Table 4. It can be clearly seen from the table that **Eu1** exhibited large K_{NR} = 12,136.93 s^{-1} compared to **Eu2** (K_{NR} = 797.27 s^{-1}). This behaviour is further reflected in the intrinsic quantum yield of **Eu1** (Q_{Eu} = 5.33) that is more than 10 times lower than that of **Eu2** (Q_{Eu} = 52.16). The value of Q_{Eu} indicates the extent of non-radiative de-activation processes in the inner and outer coordination spheres of the Ln(III) ion. The Eu(III) emission is more efficient in **Eu2** CP due to the presence of chelating TTA units that protect the Eu(III) center efficiently from coordinating water molecules that lead to de-activation processes. Furthermore, the high values of Ω_2 *viz.* 18.05 × 10^{-20} cm^2 and 22.29 × 10^{-20} cm^2 for **Eu1** and **Eu2**, respectively, imply that the Eu(III) ions in the CPs are in a highly polarizable chemical environment, which further leads to higher values of R_{21}. The higher Ω_2 value of **Eu2** compared to **Eu1** could be attributed to strong delocalization of the asymmetric β-diketonate oxygen charge around Eu(III) inside the coordination sphere.[44] Finally, the calculated Ω_4 parameter is related to long-range effects such as NCIs (HB, π–π stacking, *etc.*) and rigidity. The high values of the Ω_4 parameter in Table 4 suggest that the Eu(III) CPs display these features as verified by the crystal structure of the polymers.

Fabrication of LED

Because of the large intrinsic quantum yield of **Eu2** CP (Q_{Eu} = 52.16), its potential application as a red phosphor in fabricating a LED was investigated.[45] First, the excitation spectrum of **Eu2** in the solid-state was studied and presented in Fig. 5a. A broad band from 300 to 420 nm is observed in addition to 4f–4f transitions of Eu(III) from $^7F_0 \rightarrow {}^5D_2$ and $^7F_0 \rightarrow {}^5D_1$ transitions at 466 and 507 nm, respectively. This means that the Eu(III) centre can be sensitized by the absorption of light between 300 and 420 nm. In fact, DHTP can absorb UV-light at 378 nm. Therefore, the Eu(III) centre can also be sensitized by using blue

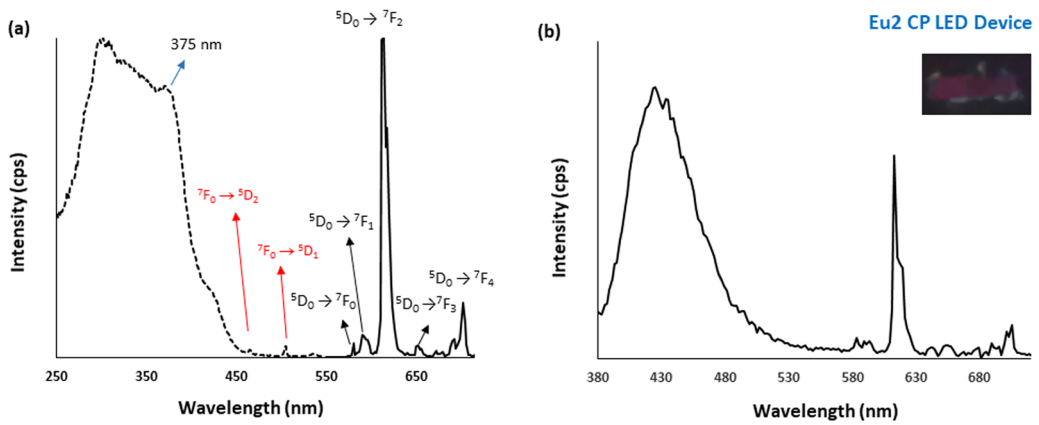

Fig. 5 (a) The excitation and emission spectra of **Eu2** CP and (b) the emission spectrum of the **Eu2**/InGaN chip device excited at 375 nm.

LED irradiation under excitation at 375 nm. Indeed, a LED was fabricated by coating a resin of 10% **Eu2** CP-silicon oil onto a blue InGaN chip.[12] The emission spectrum of the **Eu2**/InGaN LED device is shown in Fig. 5b. It shows a combination of blue emission from the InGaN chip and a red luminescence from **Eu2** CP. Interestingly, the CIE 1931 chromaticity coordinates exhibit a considerable shift of the colour coordinates of **Eu2** from (0.668, 0.325) to (0.437, 0.185) when doped on the blue chip. A simple colour detection under a UV lamp reveals the emission of pink light from the LED (Fig. 5b inset). The red light from Eu(III) has mixed with the blue light from the InGaN chip to generate the pink light from the chip device. As a result, the **Eu2** coordination polymer is promising for application as a red phosphor in fabricating LEDs.

Conclusions

Novel Eu(III) CPs were successfully synthesized and characterized. The Eu(III) polymer: $[Eu_2(DHTP)(TTA)_4(DMF)_2(MeOH)_2]_n$ (**Eu2**) exhibited a large luminescence intrinsic quantum yield of 52% and high thermal stability up to 170 °C. A simple LED was fabricated by coating a resin of 10% **Eu2** CP-silicon onto a blue InGaN chip. A pink light emission was observed from the device.

Conflicts of interest

The authors have no conflicts of interest to declare.

Acknowledgements

NKAl-R and MSK acknowledge His Majesty's Trust Fund for Strategic Research (Grant No. SR/SQU/SCI/CHEM/21/01) and the Ministry of Higher Education, Research and Innovation (MoHERI) (Grant No. RC-RG/SCI/CHEM/23/01) for funding. We thank Sultan Qaboos University, Oman for financial support. NAl-R thanks SQU for a PhD scholarship and RI thanks HM's Trust Fund for a postdoctoral fellowship.

References

1 B. Xu, L. Yan, H.-M. Hu, C. Bai, L.-L. Xue and S. He, *J. Solid State Chem.*, 2020, **288**, 121424–121434.
2 C. Marchal, Y. Filinchuk, X.-Y. Chen, D. Imbert and M. Mazzanti, *Chem. – Eur. J.*, 2009, **15**, 5273–5288.
3 M.-L. Ma, J.-H. Qin, C. Ji, H. Xu, R. Wang, B.-J. Li, S.-Q. Zang, H.-W. Hou and S. R. Batten, *J. Mater. Chem. C*, 2013, **1**, 4634–4639.
4 B. Gao, L. Fang and J. Men, *Polymer*, 2012, **53**, 4709–4717.
5 Y.-H. Han, C.-B. Tian, Q.-H. Li and S.-W. Du, *J. Mater. Chem. C*, 2014, **2**, 8065–8070.
6 Z. S. Al-Farsi, A. Al-Rashdi and N. K. Al-Rasbi, *Polyhedron*, 2016, **117**, 552–560.
7 J. Yang, G.-D. Xie, X.-F. Chen, D. Wu, X.-M. Lin, G. Zhang and Y.-P. Cai, *CrystEngComm*, 2015, **17**, 1326–1335.
8 C. F. Qiao, Y. Zhao, Y. Ren, X. Gao, M. Zhang, C. Zhou, G. Zhang and S. Chen, *J. Solid State Chem.*, 2019, **270**, 443–449.
9 S. Wang, Q. Sun, B. Devakumar, J. Liang, L. Sun and X. Huang, *J. Lumin.*, 2019, **209**, 156–162.
10 X.-Q. Song, H.-H. Meng, Z.-G. Lin and L. Wang, *ACS Appl. Polym. Mater.*, 2020, **2**(4), 1644–1655.
11 Y. Kubo and R. Nishiyabu, *Polymer*, 2017, **128**, 257–275.
12 T. Koizuka, K. Yanagisawa, Y. Hirai, Y. Kitagawa, T. Nakanishi, K. Fushimi and Y. Hasegawa, *Inorg. Chem.*, 2018, **57**, 7097–7103.
13 F. A. de Jesusa, B. V. Santanaa, G. F. da Cunha Bispob, C. I. da Silva Filhoc, S. A. Júniorc, M. E. Giroldo Valériob, J. M. Almeida Caiutd and V. H. Vitorino Sarmento, *Polymer*, 2019, **181**, 121767.
14 P. Thuery and B. Masc, *Cryst. Growth Des.*, 2010, **10**(8), 3626–3631.
15 M. Latva, H. Takalo, V. M. Mukkala, C. Matachescu, J.-C. Rodriguez-Ubis and J. Kankare, *J. Lumin.*, 1997, **75**, 149–169.
16 A. E. Sedykh, D. G. Kurth and K. Müller-Buschbaum, *Eur. J. Inorg. Chem.*, 2019, 4564–4571.
17 K. P. Kepp, *Inorg. Chem.*, 2016, **55**, 9461–9470.
18 J. Ma, F.-L. Jiang, L. Chen, M.-Y. Wu, S.-Q. Zhang, K.-C. Xiong, D. Han and M.-C. Hong, *CrystEngComm*, 2012, **14**, 6055–6063.
19 J. D. Einkauf, J. M. Clark, A. Paulive, G. P. Tanner and D. T. de Lill, *Inorg. Chem.*, 2017, **56**, 5544–5552.
20 A.-J. Huang, L.-H. Leng, D.-Q. Xin and S.-C. Ding, *Inorg. Nano-Met. Chem.*, 2020, 1–8.
21 A. Lämmermann, I. Szatmári, F. Fülöp and E. Kleinpeter, *J. Phys. Chem. A*, 2009, **113**, 6197–6205.
22 A. Haque, K. M. Alenezi, M. S. Khan, W.-Y. Wong and P. R. Raithby, *Chem. Soc. Rev.*, 2023, **52**, 454–472.
23 R. Ilmi, D. Zhang, L. Tensi, H. Al-Sharji, N. K. Al Rasbi, A. Macchioni, L. Zhou, W.-Y. Wong, P. R. Raithby and M. S. Khan, *Dyes Pigm.*, 2022, 110300.
24 R. Ilmi, J. Yin, J. D. L. Dutra, N. K. Al Rasbi, W. F. Oliveira, L. Zhou, W.-Y. Wong, P. R. Raithby and M. S. Khan, *Dalton Trans.*, 2022, **51**, 14228–14242.
25 X. Lucas, C. Estarellas, D. Escudero, A. Frontera, D. Quiñonero and P. M. Deyà, *Chem. Phys. Chem.*, 2009, **10**, 2256–2264.
26 Stoe & Cie, *X-AREA, version 1.30: Program for the acquisition and analysis data*, Stoe & Cie GmbH, Darmatadt, Germany, 2005.
27 Stoe & Cie, *X-RED, version 1.28b: Program for data reduction and absorption correction*, Stoe & Cie GmbH, Darmatadt, Germany, 2005.
28 G. M. Sheldrick, *SHELX97. Program for crystal structure solution and refinement*, University of Göttingen, Germany, 1997.
29 L. J. Farrugia, *J. Appl. Crystallogr.*, 1999, **32**, 837–838.
30 C. F. Macrae, P. R. Edgington, P. McCabe, E. Pidcock, G. P. Shields, R. Taylor, M. Towler and J. van de Streek, *J. Appl. Crystallogr.*, 2006, **39**, 453–457.

31 R. Ilmi, W. Sun, J. D. L. Dutra, N. K. Al-Rasbi, L. Zhou, P.-C. Qian, W.-Y. Wong, P. R. Raithby and M. S. Khan, *J. Mater. Chem. C*, 2020, **8**, 9816–9827.
32 J. Li, X. Zhang, B. Yue, A. Wang, L. Kong, J. Zhou, H. Chu and Y. Zhao, *Crystals*, 2017, **7**, 139.
33 B. C. Barja, A. Remorino, M. J. Roberti and P. F. Aramendia, *J. Argent. Chem. Soc.*, 2005, **93**, 81–96.
34 J. Ye, J. Zhang, G. Ning, G. Tian, Y. Chen and Y. Wang, *Cryst. Growth Des.*, 2008, **8**, 3098–3106.
35 J. D. Einkauf, T. T. Kelley, B. C. Chan and D. T. de Lill, *Inorg. Chem.*, 2016, **55**, 7920–7927.
36 S. Tobita, M. Arakawa and I. Tanaka, *J. Phys. Chem.*, 1985, **89**(26), 5649–5654.
37 R. Ilmi, M. S. Khan, Z. Li, L. Zhou, W.-Y. Wong, F. Marken and P. R. Raithby, *Inorg. Chem.*, 2019, **58**(13), 8316–8331.
38 C. Serre, F. Millange, J. Marrot and G. Férey, *Chem. Materials*, 2002, **14**, 2409–2415.
39 N. K. Al-Rasbi, H. Adams and F. O. Suliman, *Dyes Pigm.*, 2014, **104**, 83–88.
40 A. Al-Bahri, A. S. Al-Zakwani, S. M. Al-Farsi and N. K. Al-Rasbi, *ChemistrySelect*, 2016, **1**, 1393–1399.
41 F. J. Steemers, W. Verboom, D. N. Reinhoudt, E. B. van der Tol and J. W. Verhoeven, *J. Am. Chem. Soc.*, 1995, **117**(37), 9408–9414.
42 R. Ilmi, S. Anjum, A. Haque and M. S. Khan, *J. Photochem. Photobiol., A*, 2019, **282**, 111968.
43 R. Ilmi, D. Zhang, J. D. L. Dutra, N. Dege, L. Zhou, W.-Y. Wong, P. R. Raithby and M. S. Khan, *Org. Electron.*, 2021, **96**, 106216.
44 I. J. Al-Busaidi, R. Ilmi, D. Zhang, J. D. L. Dutra, W. F. Oliveira, N. K. Al Rasbi, L. Zhou, W.-Y. Wong, P. R. Raithby and M. S. Khan, *Dyes Pigm.*, 2022, **197**, 109879.
45 L. Armelaoa, S. Quicib, F. Barigelletti, G. Accorsic, G. Bottarod, M. Cavazzinib and E. Tondelloe, *Coord. Chem. Rev.*, 2010, **254**, 487–505.